Phase-separated liposomes hijack endogenous lipoprotein transport and metabolism pathways to target subsets of endothelial cells in vivo

Arias Alpizar, G.; Papadopoulou, P.; Rios, X.; Pulagam, K.R.; Moradi, M.A.; Pattipeiluhu, R.; ... ; Campbell, F.

Citation

Phase-Separated Liposomes Hijack Endogenous Lipoprotein Transport and Metabolism Pathways to Target Subsets of Endothelial Cells In Vivo

Gabriela Arias-Alpizar, Panagiota Papadopoulou, Xabier Rios, Krishna Reddy Pulagam, Mohammad-Amin Moradi, Roy Pattipeiluhu, Jeroen Bussmann, Nico Sommerdijk, Jordi Llop, Alexander Kros,* and Frederick Campbell*

Plasma lipid transport and metabolism are essential to ensure correct cellular function throughout the body. Dynamically regulated in time and space, the well-characterized mechanisms underpinning plasma lipid transport and metabolism offers an enticing, but as yet underexplored, rationale to design synthetic lipid nanoparticles with inherent cell/tissue selectivity. Herein, a systemically administered liposome formulation, composed of just two lipids, that is capable of hijacking a triglyceride lipase-mediated lipid transport pathway resulting in liposome recognition and uptake within specific endothelial cell subsets is described. In the absence of targeting ligands, liposome-lipase interactions are mediated by a unique, phase-separated ("parachute") liposome morphology. Within the embryonic zebrafish, selective liposome accumulation is observed at the developing blood-brain barrier. In mice, extensive liposome accumulation within the liver and spleen – which is reduced, but not eliminated, following small molecule lipase inhibition – supports a role for endothelial lipase but highlights these liposomes are also subject to significant "off-target" by reticuloendothelial system organs. Overall, these compositionally simplistic liposomes offer new insights into the discovery and design of lipid-based nanoparticles that can exploit endogenous lipid transport and metabolism pathways to achieve cell selective targeting in vivo.

1. Introduction

All cells rely on plasma lipid transport to maintain a correct intracellular balance of essential and non-essential fatty acids. This requires the dynamic regulation of the secretion, transport, and metabolism of water-insoluble fats throughout the body. Often packaged, secreted, and transported as nanometer-sized, solid lipid particles (i.e., lipoproteins), many of the biological mechanisms underpinning endogenous plasma lipid transport and metabolism are now well understood.[1] Despite compositional and structural similarities of lipoproteins and synthetic lipid-based nanoparticles, however, there are currently few examples of synthetic lipid-based nanoparticles that explicitly hijack endogenous lipid transport mechanisms to achieve target cell specificity. One notable example, however, is Onpattro – a clinically approved lipid nanoparticle (LNP)-RNAi therapy used to treat polyneuropathies resulting from transthyretin-mediated amyloidosis (hATTR). In this case, selective recognition

G. Arias-Alpizar, P. Papadopoulou, R. Pattipeiluhu, J. Bussmann, A. Kros, F. Campbell[+]
Supramolecular and Biomaterials Chemistry
Leiden Institute of Chemistry
Leiden University
P.O. Box 9502, Leiden 2300, The Netherlands
E-mail: a.kros@chem.leidenuniv.nl; f.campbell@nanovationtx.com

G. Arias-Alpizar, J. Bussmann
Division of BioTherapeutics
Leiden Academic Centre for Drug Research
Leiden University
P.O. Box 9502, Leiden 2300, The Netherlands

X. Rios, K. R. Pulagam
CIC biomaGUNE
Basque Research and Technology Alliance (BRTA)
San Sebastián 20014, Spain

M.-A. Moradi, J. Llop
Materials and Interface Chemistry
Department of Chemical Engineering and Chemistry
Eindhoven University of Technology
P.O. Box 513, Eindhoven 5600, The Netherlands

N. Sommerdijk
Department of Biochemistry
Radboud Institute for Molecular Life Sciences
Radboud University Medical Center
Nijmegen 6525, The Netherlands

and uptake within target hepatocytes rely on the adsorption of soluble apolipoprotein E (apoE) to the surface of circulating LNPs. This, in turn, guides Onpattro to low-density lipoprotein receptors (LDLr) that are heavily expressed on the sinusoidal surface of hepatocytes.[2,3] This clinically relevant lipid nanoparticle formulation highlights the enticing, but largely unexplored,[4,5] potential of exploiting endogenous lipid transport to guide nanoparticles to specific tissues and cells within the body.

The three main plasma lipid transport forms are free fatty acids (FAs), triglycerides (TGs), and cholesteryl esters (CEs).[1] Free FAs are generally transported as a complex with serum albumin, whereas TGs and CEs are transported within the core of plasma lipoproteins – solid lipid particles surrounded by a lipid monolayer rich in phospholipids and stabilized by apolipoprotein(s). The five major classes of lipoproteins are chylomicrons (secreted by the intestine, size: 100–1000 nm); very-low-density lipoproteins (VLDLs, secreted by the liver, size: 50–200 nm), intermediate and low-density lipoproteins (IDLs and LDLs, lipoprotein metabolites enriched in cholesterol, and, at high levels, associated with atherogenic disorders;[6,7] size: 20–50 nm) and high-density lipoproteins (HDLs, involved in reverse cholesterol transport,[8] size: 8–12 nm). In the case of VLDL and chylomicrons, a single, surface-bound apolipoprotein B – apoB100 or apoB48 respectively – stabilizes each secreted lipoprotein. HDLs, in contrast, are stabilized by apolipoprotein A-I (apoAI).[9,10]

Once secreted into the bloodstream, soluble and exchangeable apolipoproteins (e.g., apoA, C, D, and E) recognize and bind to the surface of a circulating lipoprotein. These apolipoproteins guide lipoproteins to specific targets within the body. For example, apoE is a ligand for LDLr, promoting uptake primarily in hepatocytes,[11] lipoprotein-bound apoC2 functions as an obligatory cofactor of lipoprotein lipase (LPL),[12,13] whereas apoA1 binds a wide range of cognate receptors and enzymes including LDLr,[14] scavenger receptor B-1 (SRB-1),[15–17] ATP-binding cassette transporters A1 (ABCA1) and G1 (ABCG1),[18–20] and endothelial lipase (EL).[21,22]

Following transport, lipoproteins are generally metabolized to release free fatty acids that are then taken up locally by cells. TG lipases are key extracellular, hydrolytic enzymes that regulate lipid metabolism throughout the body. The three main members of the TG lipase family are LPL,[23] hepatic lipase (HL),[24] and EL[21,25] (encoded by the human genes *LPL*, *LIPC*, and *LIPG* respectively). All three share significant structural homology, including a conserved catalytic triad of amino acids (serine, aspartate, and histidine), as well as conserved heparin and lipoprotein binding domains.[21,25] LPL is predominantly synthesized in adipose tissue, heart, and skeletal muscle; HL in hepatocytes; and EL in vascular endothelial cells.[21] Once expressed, TG lipases are secreted and actively transported (in the case of LPL and HL) to the local endothelium where they anchor to heparan sulfate proteoglycans (HSPG) via electrostatic interactions.[22] As hydrolytic enzymes, LPL primarily hydrolyzes TGs,[26] HL–TGs and

phospholipids,[24,27] and EL–phospholipids.[21] Substrate specificity is determined by sequence variation in the lid region of each enzyme.[21,28,29] However, whereas LPL and HL metabolize fats primarily derived from VLDL and chylomicrons, the principle function of EL is the regulation of HDL metabolism via interactions with apoA-1.[21,30–33] In addition, all three TG lipase family members are capable of internalizing lipoproteins via proteoglycan- or receptor-mediated pathways in a non-enzymatic fashion.[22,34,35]

Herein, we describe a systemically administered liposome formulation, composed of just two lipids, that preferentially targets a specific subset of endothelial cells in vivo. Most notably, these liposomes accumulate at the brain endothelium of an embryonic zebrafish. Mechanistically, we show that target selectivity is linked to the ability of these liposomes to interact with endogenous (endothelial) lipase, although whether cell selectivity arises as a result of direct (e.g., non-enzymatic lipase-mediated recognition and uptake) or indirect (i.e., lipase mediated metabolism distant to target cellular uptake) lipase engagement is not yet clear. With no additional "targeting" functionality, lipase-liposome interactions are mediated through a unique, phase-separated ("parachute") liposome morphology, onto the surface of which preferentially adsorb apolipoproteins A1, A4, and E. Within 6–8 weeks-old mice, liposomes predominantly accumulate within the liver and spleen. While in the liver, we show liposome accumulation is in part mediated by lipase interaction, these observations ultimately reaffirm that the capacity of these RES organs to clear nanoparticles from circulation is both proficient and mechanistically multipronged.

2. Results

2.1. PAP3 Liposomes Accumulate at the Brain Endothelium of Embryonic Zebrafish

Zebrafish embryos are convenient, accurate, and cost-effective animals to study the behavior and pharmacokinetics of nanoparticles in vivo,[36,37] to assess and predict key nanoparticle-liver interactions within higher vertebrates[38,39] and to identify endogenous biological pathways underpinning nanoparticle fate in vivo.[38–40] From a preliminary screen of i.v. administered liposomes, we unexpectedly observed selective accumulation of a liposomal formulation, PAP3, within the head region of a three-day-old (≈78 hpf) zebrafish embryo (**Figure 1**a,b). PAP3 liposomes (size: ≈120 nm) were composed of an equimolar mixture of just two lipids: a novel synthetic lipid, 2-hydroxy-3-oleamidopropyl oleate (DOaG), and naturally occurring, 1,2-distearyl-*sn*-glycero-3-phosphocholine (DSPC) (Figure 1c). These liposomes contained no additional targeting functionality. Looking closely within the head region of the zebrafish embryo, PAP3 liposomes clearly accumulated within some (e.g., mesencephalic vein (MsV), mesencephalic artery (MsA), middle mesencephalic central artery (MMCtA), middle cerebral vein (MCeV), primordial hindbrain channels (PHBC) and cerebral arteries (CtAs)), but not all (e.g., dorsal longitudinal vein (DLV), primordial midbrain channel (PMBC)) blood vessels and capillaries within the embryo head (Figure 1d). The specific blood vessels and capillaries in which PAP3 liposomes accumulated have been previously

N. Sommerdijk
Electron Microscopy Centre
Radboudumc Technology Center Microscopy
Radboud University Medical Center
Geert Grooteplein Zuid 28, Nijmegen 6525, The Netherlands
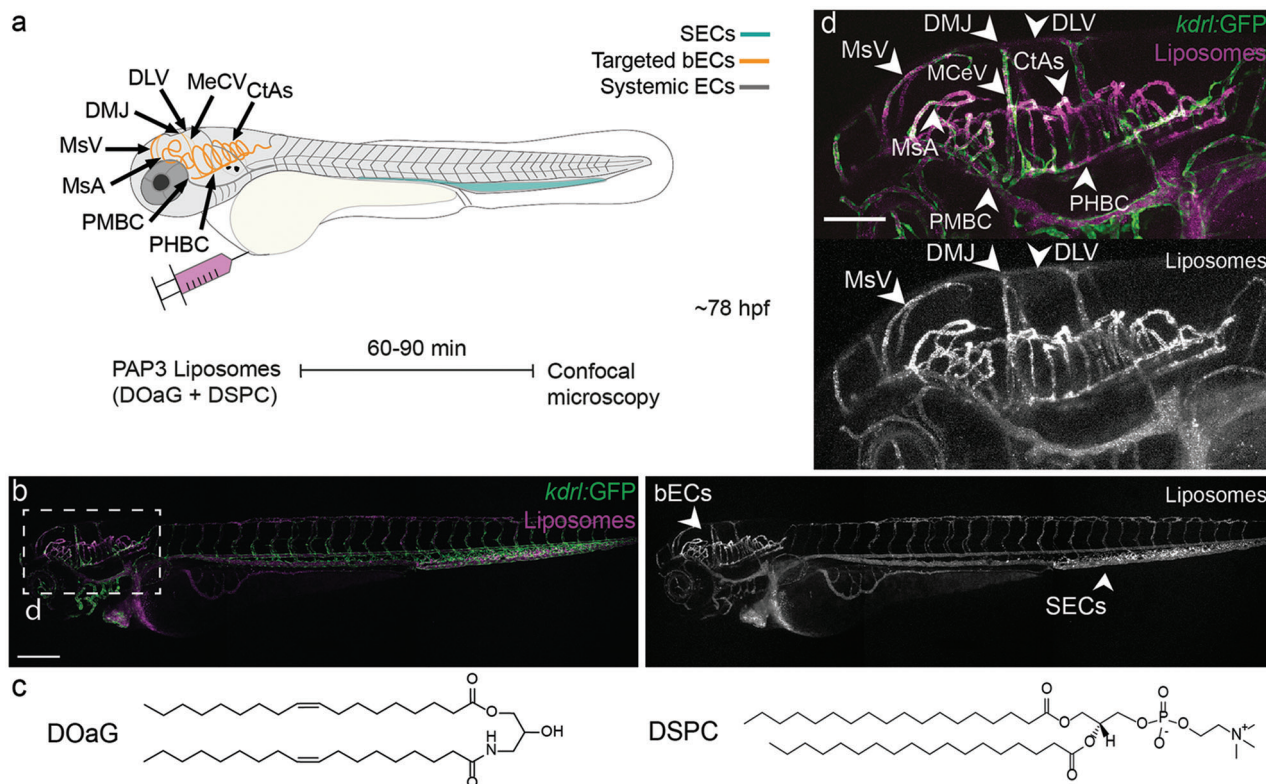
Figure 1. Biodistribution of PAP3 liposomes within zebrafish embryos (78 hpf). a) Schematic zebrafish larvae in lateral (whole-body) view, showing the site of microinjection and key cranial vessels. Fluorescently labeled liposomes are imaged with confocal microscopy after 60–90 min. The vasculature is as follows, liposome targeted bECs in yellow and systemic endothelium in dark gray, scavenger endothelial cells (SECs) in cyan, at ≈78 h post-fertilization (hpf). b) Biodistribution (10x magnification, lateral view) of PAP3 liposomes within a Tg(kdrl:GPF) zebrafish embryo at 1.5 h post-injection (hpi). c) Chemical structure of lipids used in the equimolar mixture for the formulation of PAP3 liposomes, DOaG, and DSPC lipids. d) Zoom of the cranial region in lateral view. bECs, brain endothelial cells; CtAs, central arteries; DLV, dorsal longitudinal vein; DMJ, dorsal midline junction; MCeV, middle cerebral vein; MsA, mesencephalic artery; MsV, mesencephalic vein; PMBC, primordial midbrain channel; PHBC, primordial hindbrain channel; SECs, scavenging endothelial cells. Liposomes formulated by extrusion (5 mM, 0.2% mol DOPE-LR). Scale bars: 200 µm (lateral view) and 100 µm (zoom).

characterized as the brain endothelium (i.e., bECs), constituting the blood-brain barrier (BBB) of the developing embryo.[41–43]

Anatomical features that regulate mammalian brain homeostasis and permeability are highly conserved in zebrafish. These features include endothelial tight junctions, maintained by specialized tight junction proteins (e.g., Claudin-5);[42,44,45] pericytes and glia cells surrounding the brain vasculature;[46,47] and the expression of substrate-specific transporters (e.g., GLUT1).[48] All these features are present and functional (as assessed by permeability assay) within the embryonic zebrafish by 3 days post-fertilization (dpf).[49] Importantly, angiogenesis within the brain of the embryonic zebrafish is temporally coupled to barriergenesis.[48] This means nascent bECs immediately express genes associated with BBB function. As such, the dynamic expression of the tight junction protein Claudin-5, encoded by *claudin5a*, has been previously used to map the developing endothelium of the embryonic zebrafish brain over time.[42,44,45,48] This simple and clear delineation of brain versus systemic endothelial cells within the head region of the embryonic zebrafish, therefore provides an ideal in vivo screening platform to assess bEC target specificity using standard fluorescence microscopy setups (**Figure 2**a and Figure S1a,b, Supporting Information).[42,44,45]

To verify selective liposome accumulation with bECs, PAP3 liposomes were administered (i.v.) within embryonic zebrafish at different developmental stages (2, 3, and 4 dpf) (Figure 2b–d). This two-day timeframe spans the onset and maturation of the embryonic BBB, most prominently within the mid- and fore-brain, following complete hindbrain vascular invasion by 48 hpf (characterized by CtA capillary loops connecting both PHBCs with the central basilar artery [BA]).[41] Accordingly, at 2 dpf, PAP3 liposomes mainly accumulated in functional bECs, within blood vessels and capillaries of the hindbrain, namely CtAs, BA, and PHBCs (Figure 2b). At 3 dpf, as blood vessels irrigate rostrally throughout the brain,[50] PAP3 liposomes accumulated within newly formed capillaries of the mid- and fore-brain (Figure 2e), as well as within the continually expanding BBB vasculature of the hindbrain (Figure 2f,h,i and Figure S1a,b, Supporting Information for a Z-stack depth color-coded of the vasculature in dorsal view). By 4 dpf, PAP3 liposomes extensively accumulated throughout the brain endothelium of the embryonic zebrafish (Figure 2d). Notably, at all developmental stages, liposomes did not drastically accumulate in systemic blood vessels (e.g., PMBC and DLV) within the head region (Figure 2g), confirming a specific preference of PAP3 liposomes for bECs at all developmental time-points. Indeed, colocalization of PAP3 liposome accumula-
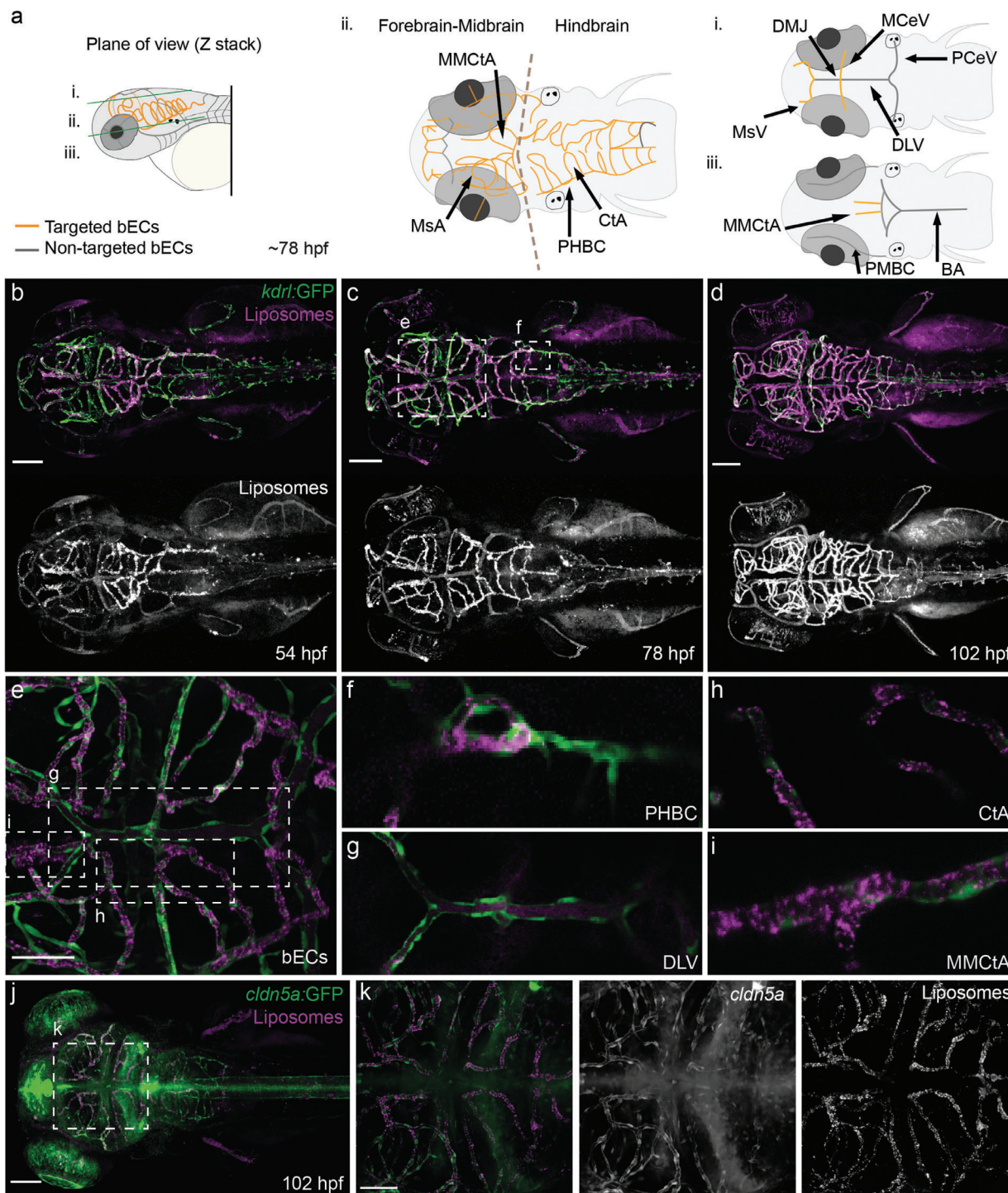
Figure 2. Biodistribution of PAP3 liposomes within the head region of zebrafish embryos. a) Schematic zebrafish larvae with key blood vessels in different planes of view. See Figure S1a,b, Supporting Information for a Z-stacks depth color-coded zebrafish vasculature. Dorsal view, showing the i) top, ii) middle, and iii) bottom layer diagram. The vasculature is as follows, targeted brain endothelial cells (bECs) in yellow and non-targeted systemic endothelium in dark gray, at ≈78 h post-fertilization (hpf). PHBC, primordial hindbrain channel; CtA, central artery; DLV, dorsal longitudinal vein; MsA, mesencephalic artery; MsV, mesencephalic vein; MMCtA, middle mesencephalic central artery. b) Biodistribution (10x magnification, dorsal view, 1.5 hpi) of PAP3 liposomes (5 mM, 0.2% mol DOPE-LR) within the head region of a Tg(*kdrl*:GFP) zebrafish embryo at 54, c) 78, and d) 102 hpf. e) High magnification view of c) (inset, 40x, zoom) showing PAP3 liposomes accumulating within bECs. f) Posterior part of the PHBC, g) DLV, h) CtA, i) MMCtA. j,k) Biodistribution of PAP3 liposomes in a Tg(*cldn5a*:GFP)[42] zebrafish embryo (102 hpf) with GFP-labeling in blood and choroid plexus brain barrier showing colocalization of *cldn5a* with fluorescent liposomes. Zoom-in of the region that includes the hindbrain vasculature and colocalization with *cldn5a* expression is shown in Figure S1c, Supporting Information. Liposomes formulated by extrusion (5 mM, 0.2 mol% DOPE-LR). Scale bars: 100 μm (dorsal view), 50 μm (tissue level).

tion and Claudin-5 expression, notably within the CtAs, MMCtA (Figure 2h,i), and MsA, was confirmed in Tg(*cldn5a*:eGFP)[42] embryos stably expressing an integrated eGFP-Claudin5a fusion protein (Figure 2j,k and Figure S1c, Supporting Information).

In addition to bEC target selectivity, PAP3 liposomes also accumulated in the tail within the caudal hematopoietic tissue (CHT) and caudal vein (CV) of the embryo (Figure 1a,b). We have previously shown that these blood vessels are composed of scavenger endothelial cells (SECs) and blood resident macrophages, equivalent to hepatic reticuloendothelial (RES) cells (i.e., liver sinusoidal endothelial cells (LSECs) and Kupffer cells (KCs)) in mammals.[38] SECs, in particular, proficiently recognize and clear anionic nanoparticles, as well as neutral DSPC liposomes, from circulation via the conserved scavenger receptors, Stabilin-1 and -2. Accordingly, systemic administration of DSPC-containing PAP3 liposomes in zebrafish mutants lacking functional scavenger receptors Stabilin-1 and Stabilin-2 (*stabilin-1*ibl3 *stabilin-2*ibl1)[39] resulted in reduced liposome accumulation within the CHT and CV of the embryo without significantly affecting bEC targeting (Figure S2, Supporting Information). This confirmed that (off-)targeting of PAP3 liposomes to RES-like cell types, but not bECs, was, at least in part, Stabilin-dependent. However, persistent liposome accumulation within blood resident macrophages of the mutant *stabilin-1/-2* double knockout embryo suggested potentially significant and competitive pathways of PAP3 RES clearance.

2.2. Cryo-TEM Revealed a Novel "Parachute" Liposome Morphology that is Essential for BBB Targeting in Embryonic Zebrafish

To rationalize bEC-liposome specificity, and in the absence of any additional targeting functionality (e.g., targeting ligands), cryogenic transmission electron microscopy (cryo-TEM) was performed to characterize PAP3 liposome ultrastructure. Unexpectedly, these images revealed a highly unusual phase-separated, "parachute" morphology, characterized by a single electron-rich protrusion within each liposomal membrane (**Figure 3a–c** and Figure S3, Supporting Information). Such parachute-like structures have been previously reported for lipid-polymer hybrid nanoparticles[51,52] propofol-containing liposomes,[53] and mRNA-encapsulated LNPs[54,55] but, to the best of our knowledge, have not been reported for purely lipidic nanoparticles. Given the flat, bilayer preference of amphipathic DSPC, the observed phase-separated protrusion was hypothesized to be rich in DOaG. Indeed, at a molecular level, DOaG is structurally very similar to diacylglycerols (DAGs) whose hydrophobicity and geometry are known to alter the spontaneous curvature of PC lipid membranes and perturb lamellar membrane structures, resulting in the formation of non-bilayer phases.[56–60]
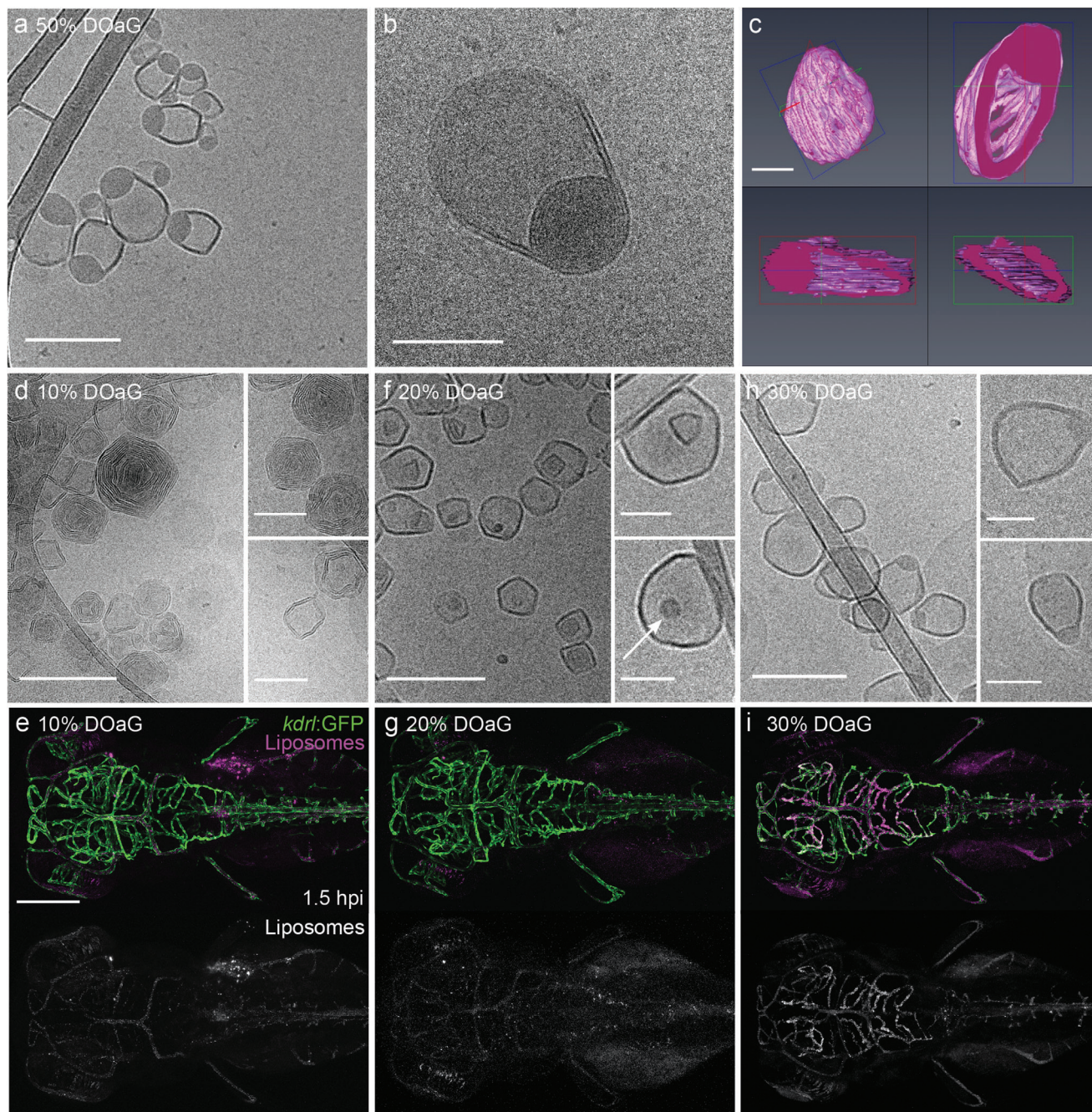
To investigate the possible association of phase separation and liposome-bEC selectivity, PAP3 liposomes were formulated at varying molar ratios (10–50 mol% DOaG) to correlate liposome morphology with in vivo biodistribution (Figure 3d–i). Of note, > 50 mol% DOaG resulted in liposome aggregation. CryoEM images of 10% DOaG liposomes (10–90 mol% DOaG-DSPC) revealed a mixture of non-spherical, bi-layered, and multilamellar particles with no evident phase separation (Figure 3d and Fig-

ure S4a, Supporting Information). 10% DOaG liposomes mostly accumulated within SECs in the CV and CHT of the embryo (Figure S5a, Supporting Information) and did not target bECs (Figure 3e). Likewise, 20% DOaG liposomes (20–80 mol% DOaG-DSPC) were predominantly non-spherical (Figure 3f and Figure S4b, Supporting Information), mainly accumulated within SECs (Figure S5b, Supporting Information) and did not target bECs (Figure 3g). However, at 20% DOaG, small electron-rich protrusions within the liposome membrane indicated a liposome formulation approaching its miscibility threshold (Figure 3f and Figure S4b, Supporting Information – white arrows). This was confirmed by the clear phase separation of 30% DOaG liposomes (30–70 mol% DOaG-DSPC) in which a single lipid protrusion was now clearly evident within each discreet liposome membrane (Figure 3h and Figure S4c, Supporting Information). 30% DOaG liposomes, as for PAP3 liposomes (i.e., 50–50 mol% DOaG-DSPC), proficiently targeted bECs of the zebrafish larvae (Figure 3i and Figure S5c, Supporting Information).

A 30 mol% DOaG miscibility threshold (within a DSPC bilayer) closely mirrors that previously reported for structurally similar DAG (i.e., 25 mol% miscibility threshold within a PC bilayer).[61] Accordingly, to better understand the molecular details of DOaG lipid that facilitate the phase separation, we replaced the amide bond in DOaG with an ester bond, resulting in the naturally occurring diacylglycerol analogue, 1,3-dioleoylglycerol (1,3-DOG). This also led to phase-separated liposomes and bEC targeting (Figure S6a–d, Supporting Information). However, creating an analogue with two amides or replacing the oleic chains with stearyl chains (Figure S6e,f, Supporting Information) resulted in lipids that cannot formulate liposomes. In addition, lipid phase separation is known to be dependent on the gel phase state of a lipid bilayer. Consequently, switching co-formulant phospholipid from saturated DSPC (phase transition temperature $[T_m]$ 55 °C) to unsaturated DOPC ($T_m = -17$ °C) resulted in liposomes (at room temperature) with no apparent phase separation and severely ablated bEC targeting (Figure S7, Supporting Information). Notably, incorporation of polyethylene glycol (PEG)-conjugated lipid (e.g., 1,2-distearoyl-sn-glycero-3-phosphatidylethanolamine DSPE-PEG-2000, 5 mol% as commonly used)[62,63] to the PAP3 liposome results in the loss of selective targeting, as observed in the zebrafish (Figure S8a,b, Supporting Information). Altogether, these experiments confirmed the critical requirement of phase-separated lipid protrusions for bEC selective liposome accumulation within the embryonic zebrafish.

2.3. PAP3 Liposome Targeting and Uptake by bECs in Zebrafish Larvae is Partially Mediated by (Endothelial) Lipase

In the absence of any additional targeting functionality (i.e., targeting ligands), we next investigated whether PAP3 liposomes could be hijacking an endogenous plasma lipid transport pathway to selectively target bECs of the embryonic zebrafish. Importantly, all major elements of mammalian plasma lipid transport and metabolism, including the expression of apolipoproteins, lipoprotein receptors (e.g., low-density lipoprotein receptor, LDLR), and hydrolytic enzymes (e.g., lipases), are present and functional in a three-day-old zebrafish embryo.[64–66] These
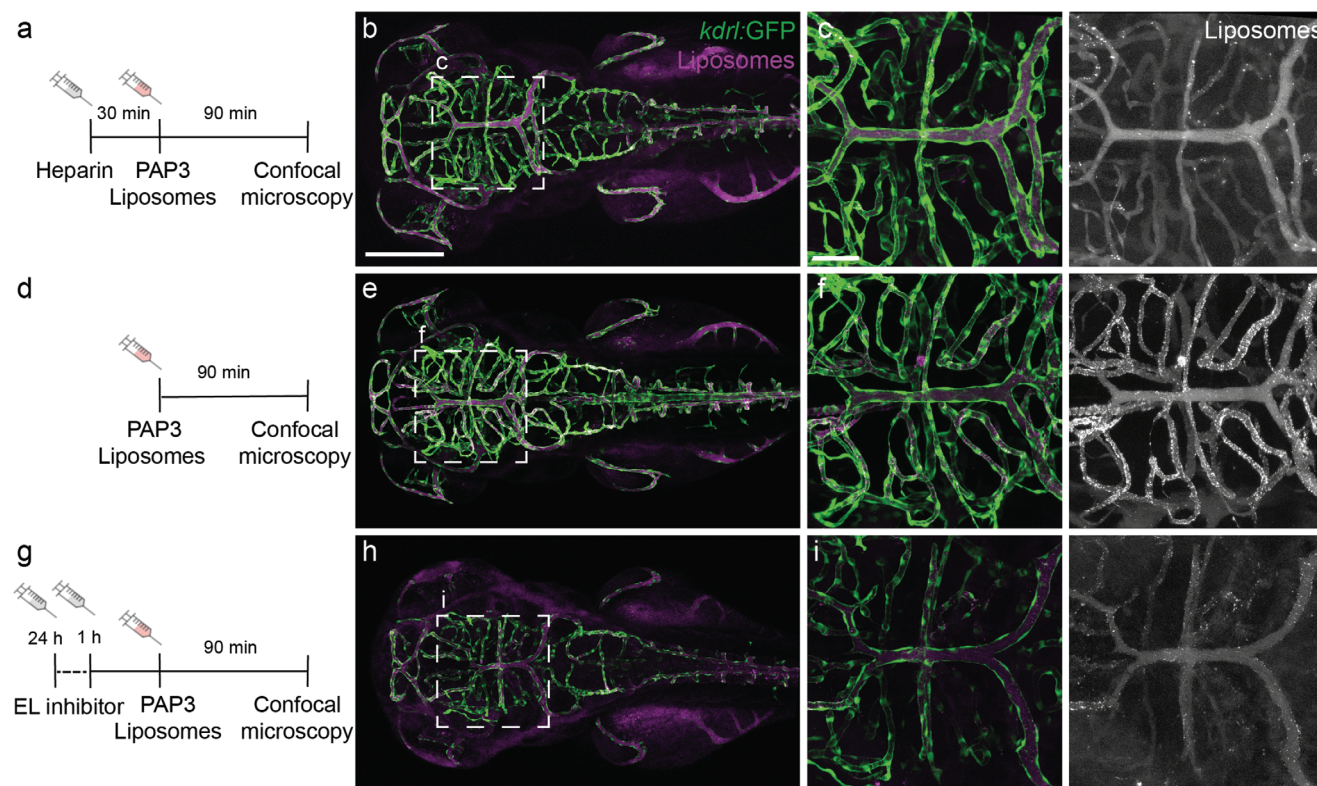
**ADVANCED
SCIENCE NEWS**

www.advancedsciencenews.com

**ADVANCED
HEALTHCARE
MATERIALS**

www.advhealthmat.de

Figure 3. Cryo-TEM of PAP3 liposomes characterized by phase separation correlates with the bECs targeting in zebrafish larvae (≈78 hpf). a,b) CryoTEM of PAP3 (50–50 mol% DOaG-DSPC) liposomes and c) 3D model of a representative PAP3 liposome reconstructed based on the electron density derived from cryo-electron tomography, demonstrating the whole body and different plane sections of the particle. CryoTEM and biodistribution (in a Tg(*kdrl*:GFP) zebrafish embryo at 1.5 hpi) of liposomes containing DSPC and d,e) DOaG 10 mol%, f,g) 20 mol%, and h,i) 30 mol%. Liposomes (5 mM, 0.2% mol DOPE-LR) described in all panels formulated by ethanol injection except panels (b) and (c) – formulated by extrusion. Scale bars: 200 nm and 100 nm for higher magnification insets for CryoTEM, 100 nm for 3D reconstruction, and 200 μm for dorsal zebrafish view.

conserved features have led to the zebrafish being used as an in vivo model to investigate various lipid disorders,[67–69] including hypertriglyceridemia, a disease caused by a malfunction in lipase-mediated plasma lipid transport and metabolism.[70]

Following secretion into the blood, the typical first step of lipoprotein-mediated plasma lipid transport is the binding of sol-uble apolipoproteins.[1] To identify serum proteins preferentially adsorbed to PAP3 liposomes, we performed a photoaffinity-based capture of the PAP3 liposome protein corona.[71] For consistency, this experiment should be performed using zebrafish serum col-lected during embryonic stages; however, given the practical diffi-culties in obtaining sufficient embryonic zebrafish serum, these

**ADVANCED
SCIENCE NEWS**

www.advancedsciencenews.com

**ADVANCED
HEALTHCARE
MATERIALS**

www.advhealthmat.de

Figure 4. bECs targeting by PAP3 liposomes is inhibited by heparin and an EL lipase inhibitor. a) Timeline of injection and imaging. b,c) Biodistribution (10x and 40x magnification) of PAP3 liposomes at 1.5 hpi, after heparin (1 nl, 50 mg ml^{-1}) administration. d) Timeline of injection and imaging. e,f) Biodistribution (10x and 40x magnification) of PAP3 liposomes, as a reference, at 1.5 hpi. g) Timeline of injection and imaging. h,i) Biodistribution (10x and 40x magnification) of PAP3 liposomes at 1.5 hpi, after a double administration (24 and 1 h prior liposome injection) of an EL inhibitor (XEN445, 1 nL of 50 µM). All zebrafish larvae, Tg(kdrl:GFP) at ≈78 hpi. Liposomes (5 mM, 0.2% mol DOPE-LR) formulated by extrusion. Scale bars: 200 µm (whole embryo) and 50 µm (tissue level).

experiments were performed in human serum and do not necessarily reflect the exact composition and abundance of serum proteins in the developing zebrafish embryo. However, functional conservation between the most abundant serum proteins in humans and zebrafish has been previously reported, including similar profiles in the apolipoproteins and complement proteins.[72] For this method, it was necessary to incorporate the photoaffinity probe, IKS02 (5 mol%),[71] within the PAP3 liposome formulation. Incorporation of this probe did not significantly alter the physicochemical properties or in vivo behavior of PAP3 liposomes (Table S1, Supporting Information). Following protein corona capture, isolation, and subsequent proteomic analysis, we identified soluble apolipoproteins as the major protein corona components of both PAP3 and control DSPC liposomes (Figure S9, Supporting Information). However, while no obvious differences in protein corona composition could easily explain the very different in vivo fates of these two liposome formulations, a significant enrichment of apoA1, A4, and apoE on the surface of both PAP3 and DSPC liposomes, at least, conformed to a lipoprotein-like transport and metabolism targeting rationale.

Given the presence of apolipoproteins on the surface of PAP3 liposomes, we next investigated the potential role of extracellular, TG lipases in the selective accumulation of PAP3 liposomes at the BBB of the zebrafish larvae. Lipases are heparin-releasable[24,73] and following heparin pre-injection (i.v.; 30 min prior to PAP3

liposome administration), PAP3 liposomes remained freely circulating with no apparent bEC targeting (**Figure 4**a–f). While this suggested TG lipase involvement, heparin is also known to bind a wide range of other proteins that could (in)directly disrupt liposome-bEC accumulation.[74] We therefore selectively inhibited TG lipase enzymatic activity using the small molecule inhibitor, XEN445.[75,76] Following XEN445 pre-treatment (1 nL, 50 µM at 24 and 1 h prior to PAP3 liposome administration), we observed a significant decrease in the bEC targeting of liposomes. This result confirmed TG lipases play a fundamental role in determining the fate of PAP3 liposomes within the embryonic fish (Figure 4g–i).

Surprisingly, however, we found that PAP3 liposomes associated with bECs were no longer heparin-releasable (**Figure 5**a–c). This indicated that PAP3 liposomes, following initial lipase interaction, were internalized by bECs. To confirm this hypothesis, we incorporated the (endosomal) pH-sensitive dye, pHrodo™, within the PAP3 liposome membrane via a phospholipid anchor[37] (see Supporting Information for characterization and Figure S10, Supporting Information for pH-dependent emission). Incorporation of up to 0.5% mol of this fluorescent probe did not significantly alter the size or bEC targeting proficiency of PAP3 liposomes (Table S1, Supporting Information).

Following liposome administration, pHrodo™-associated fluorescence was clearly observed within bECs, for example, CtAs
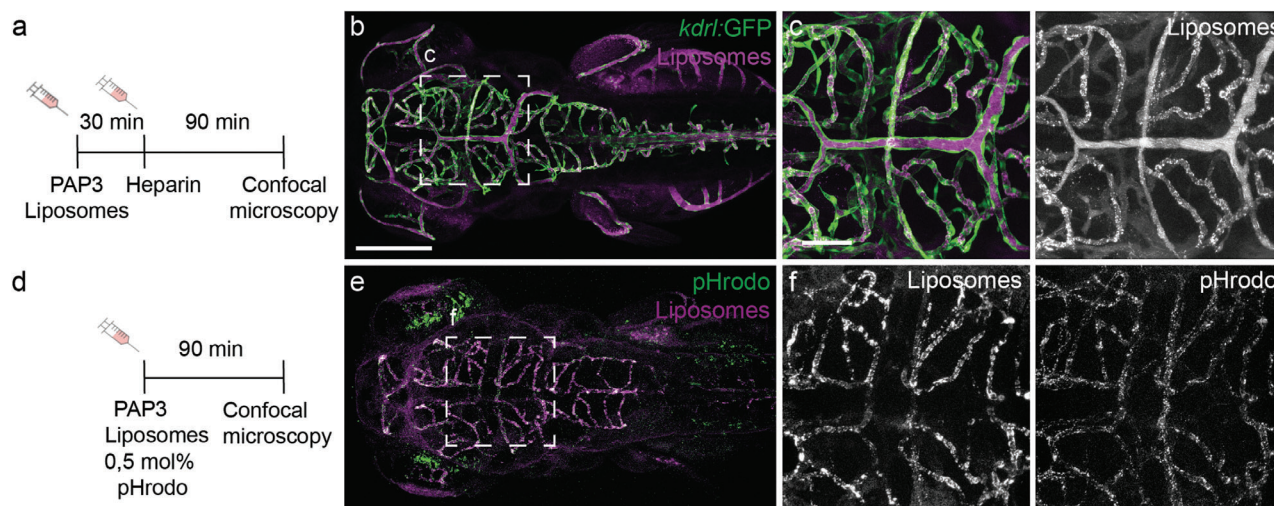
Figure 5. Internalization of PAP3 in zebrafish bECs. a) Timeline of injection and imaging. b,c) Biodistribution (10x and 40x magnification) of PAP3 liposomes (5 mM, 0.2 mol% DOPE-LR) after post-administration of heparin (1 nl, 50 mg ml^{-1}) in a Tg(kdrl:GFP) zebrafish embryo at 1.5 hpi. d) Timeline of injection and imaging. e,f) Biodistribution of PAP3 liposomes (10 mM), containing 0.5 mol% of pH-sensitive DOPE-pHrodo (green/grey) to indicate endocytosis and 0.5 mol% of non-sensitive pH dye DOPE-NBD (magenta/grey) to label liposomes, in an AB/TL zebrafish embryo at 1.5 hpi. All zebrafish larvae at ≈78 hpi. Liposomes formulated by extrusion. Scale bars: 200 µm (whole embryo) and 50 µm (tissue level).

and MMCtA, but not the systemic endothelium, for example, DLV or PMBC (Figure 5d-f), mirroring the observed biodistribution of PAP3 liposomes and confirming PAP3 liposomes are endocytosed by bECs following initial lipase-liposome interaction.

2.4. PAP3 Liposomes Accumulate within the Liver and Spleen in Mice

Finally, we quantified the dynamic biodistribution of systemically administered PAP3 liposomes in 6–8 weeks-old male mice. For these experiments, both XEN445 pre-treated (30 mg kg^{-1} XEN445 orally b.i.d. for 9 days prior to liposome administration) and untreated mice were used. As positron emission tomography (PET) tracer, a non-exchangeable ^{64}Cu (T$_{1/2}$ = 12 and 7 h) radionuclide was incorporated within the PAP3 liposome formulation, chelated via the lipid-NOTA conjugate, NOTA-Bz-SCN-C18 (0.2% mol). Based on "cold" experiments using stable Cu isotopes, the incorporation of this lipid and/or Cu chelation protocol did not affect the physicochemical properties, morphology, and/or bEC targeting proficiency of PAP3 liposomes in embryonic zebrafish (Figure S11 and Table S1, Supporting Information). Of note, phase separation on PAP3 liposomes is also maintained upon incubation in mouse serum (Figure S12, Supporting Information). Following tail vein injection (2845 ± 185 and 2480 ± 260 kBq/100 µL, XEN445 treated and non-treated mice respectively; n = 2 per group), PET scans were obtained, from 1 min to 6 h post-injection (hpi), to visualize liposome biodistribution (**Figure 6**a). These values were corroborated through ex vivo radioanalysis (% ID/g, n = 3) of the (major) organs (heart, brain, liver, spleen, kidneys, lungs, stomach, and testes) and blood, following cardiac perfusion and organ collection at 10 min, 2 h, and 6 hpi (Figure 6b,c and Figure S13, Supporting Information). This data revealed rapid and extensive liposome accumulation within the murine liver (≈53% ID/g, 10 min post-injection) and spleen (≈106% ID/g) with low levels of PAP3 liposome accumulation
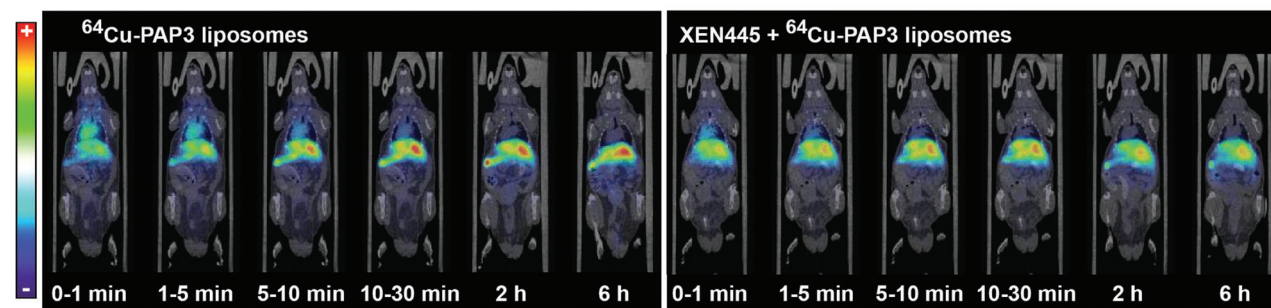
in all other organs. Following XEN445 pre-treatment (n = 3 per time point), however, a significant decrease in liposome accumulation within the murine liver, but not the spleen, was observed (Figure 6c).

This reduction in PAP3 liposome liver accumulation, following small molecule EL inhibition, confirmed at least a partial role for (endothelial) lipase in determining the fate of systemically administered PAP3 liposomes in mice. However, the failure of XEN445 to reduce liposome uptake in the spleen, as well as negligible PAP3 liposome accumulation in other EL-expressing organs (e.g., lungs and testes), was equally indicative of significant "off-target" and lipase-independent pathways of PAP3 liposome processing within RES organs of the mouse. As observed in the zebrafish embryo (Figure 1b), these "off-target" interactions in the murine liver and spleen are most likely mediated by scavenging cell types, namely LSECs, KCs, and splenic macrophages,[77,78] and these interactions are, in turn, mediated by a distinct array of receptors and enzymes, including Stabilins, class B scavenger receptors, ATP-binding cassette transporters, as well as TG lipases. To this end, it is noteworthy that apoA1-decorated nanobiologics have been specifically developed to preferentially target myeloid cells, notably in the liver and spleen.[79–81]
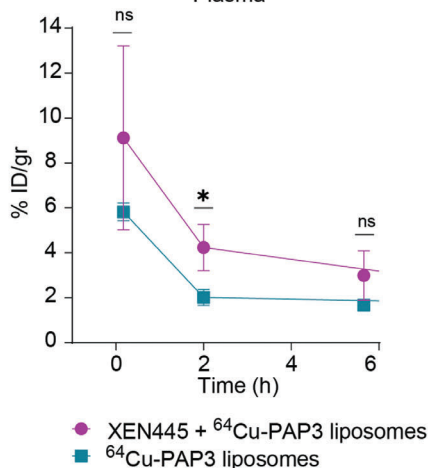
3. Discussion and Conclusion

Herein, we describe a liposome formulation, consisting of just two lipids, that is capable of hijacking an endogenous lipase-mediated pathway of lipid transport and metabolism to selectively target, and be taken up by, specific subsets of endothelial cells. While lipases, in particular small secretory phospholipase A$_2$ (sPLA2), have been previously exploited to achieve localized, stimuli-responsive drug release within target tissues (e.g., solid tumors),[82,83] lipid nanoparticle targeting of TG lipases has, to the best of our knowledge, not been described before.
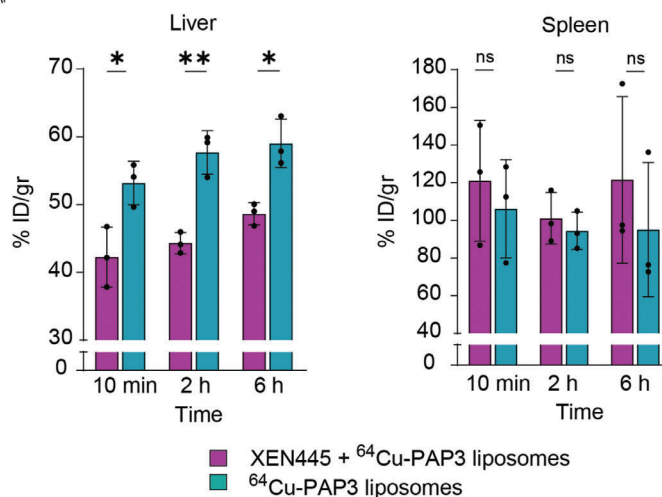
**ADVANCED
SCIENCE NEWS**

www.advancedsciencenews.com

**ADVANCED
HEALTHCARE
MATERIALS**

www.advhealthmat.de

Figure 6. Biodistribution of radiolabeled PAP3 liposomes in mice. a) Representative positron emission tomography (PET) images (coronal projections) obtained at 0–1, 1–5, 5–10, 10–30 min, and 2 and 6 h after injection of radiolabeled PAP3 liposomes containing 0.2 mol% of ^{64}Cu-NOTA-Bz-SCN-C18 in 6–8 weeks male mice treated (or not treated) with XEN445 (30 mg kg^{-1} orally, b.i.d. for 9 days) prior to liposomal injection ($n = 2$ per group and timepoint). PET images have been co-registered with representative CT slices for anatomical localization of the radioactive signal. b) Ex vivo gamma radiation counter of plasma in mice treated (or not treated) with XEN445. Concentration of radioactivity in plasma at 10 min, 2h, and 6h after i.v. administration of radiolabeled PAP3 liposomes ($n = 3$ per time point). c) Ex vivo gamma radiation counter of liver and spleen in mice treated (or not treated) with XEN445 at 10 min, 2h, and 6h after i.v. administration of radiolabeled PAP3 liposomes ($n = 3$ per group and time point). Statistical significance was evaluated using a two-tailed unpaired Student's t-test. ns: not significant ($p > 0.05$). Significantly different $*p < 0.05$, $**p < 0.01$; $***p < 0.001$. Exact p-values for b: 0.2379, 0.0242, and 0.1095. Exact p-values for c: 0.0259, 0.0029, and 0.0103 at 10 min, 2 h, and 6 h respectively for the liver and 0.5668, 0.5323, and 0.4659 for the spleen.

Lacking any additional targeting functionality, lipase recognition of PAP3 liposomes is mediated through a unique phase-separated, "parachute" morphology. Such extreme phase-separated morphologies have not been described before for purely lipid nanoparticles. The discrete lipid-rich protrusion of each liposome resembles, in both structure and size, a solid lipid nanoparticle (i.e., lipoprotein-like) and, as for analogous DAG/PC lipid mixtures, is likely characterized by increased stress on the bent membrane and increased surface hydrophobicity.[84,85] Although stable in water and tris buffer (Figure S14 and Table S1, Supporting Information), PAP3 liposomes tend to aggregate in physiologically relevant saline-containing buffers (Table S1, Supporting Information). This is in line with observations showing that increased DAG concentrations in PC bilayers decrease the ability of PC to coordinate sodium ions.[86] However, PAP3 liposomes are stable in serum (Figure S12, Supporting Information). Presumably, this is due to the rapid adsorption of soluble apolipoproteins (apoA1, A4, and E) to the liposome

surface, as is required for the stabilization of endogenously secreted lipoproteins.[1] While greater molecular understanding is required as to how these lipid-rich, phase-separated protrusions are stably incorporated within the PAP3 liposome membrane, their compositional simplicity, unique morphology, and unprecedented in vivo behavior provide an important proof-of-concept of a selective, lipase-mediated uptake pathway in vivo.

A key outstanding question is the precise mechanism of PAP3 liposome recognition and uptake within endothelial cells following lipase interaction. Here, we propose three plausible pathways. Pathway 1 – TG lipase binds to and directly internalizes PAP3 liposomes via cell surface proteoglycans (e.g., HSPG). This non-enzymatic, lipase-mediated pathway of endogenous lipoprotein uptake is known to be particularly proficient in the case of lipase-mediated uptake of HDL particles.[22,34] Pathway 2 – TG lipase binds to PAP3 liposomes and acts as a bridging molecule to a secondary receptor on the same cell, for example, apoER2, LRP1. Lipase-mediated bridging interactions are also known to

**ADVANCED
SCIENCE NEWS**

www.advancedsciencenews.com

**ADVANCED
HEALTHCARE
MATERIALS**

www.advhealthmat.de

facilitate lipoprotein intracellular uptake.[22,34,87] Pathway 3 – TG lipase binds to and enzymatically remodels PAP3 liposomes. Released PAP3 liposome metabolites are then recognized and internalized by alternative receptors expressed on target cells.

In zebrafish embryos, liposome selectivity for TG lipases is represented by bEC-specific targeting, particularly for EL and LPL over HL. Expression of EL and LPL within the head of the zebrafish embryo is high from 2 to 4 dpf.[88,89] Together with the observed prevalence of ApoA1 - a cofactor of EL – on the PAP3 liposome surface (Figure S9, Supporting Information) and XEN445 being 50–100 fold more selective inhibitor of EL (IC_{50} = 237 nM) over LPL (IC_{50} = 20 μM) and HL (IC_{50} = 9.5 μM).[75] This strongly suggests that PAP3 liposomes preferentially hijack an EL-mediated pathway of endogenous lipoprotein recognition and metabolism.[21,31] We cannot however exclude the recognition of PAP3 liposomes similarly by other lipases, namely lipoprotein lipase (LPL) and hepatic lipase (HL) and by cell types other than endothelial cells due to competing interactions. In mice, EL expression is dynamically restricted in both time and space and is particularly high between embryonic stages E8.5 and E11.5 (but not later[90]) within the developing murine brain. In healthy adults, EL expression is mainly restricted to the lungs, liver, spleen, testes, and ovaries (during pregnancy) and is particularly high in the placenta of pregnant mice.[21,25,90,91] A similar restricted pattern of EL expression has been reported in humans.[21]

Here, it is important to mention the significant decrease of PAP3 liposome uptake in the mouse liver after XEN445 treatment. This signifies the uptake acts – at least partially – as a liposome clearance mechanism via a lipase-mediated pathway. While other pathways, involving lipoprotein and more general scavenger receptors in hepatocytes and liver sinusoidal endothelial cells, as well as macrophage uptake via opsonization processes, are well established as lipid nanoparticle clearance mechanisms,[77] the role of TG lipases on nanoparticle clearance pathways, to our knowledge, has not been described before. However, in addition to the selective lipase-mediated clearance/uptake pathways, the significant competing off-target interactions by the liver and spleen have to be addressed and minimized to fully exploit this system. To this end, it will be fascinating to see if EL-mediated liposome targeting can be enhanced via local PAP3 liposome administration and/or dietary control of lipase expression.

Finally, this work again highlights the unique opportunities the zebrafish embryo can offer within nanomedicine discovery and development pipelines. Beyond the benefits of size, transparency, fecundity, and ease of genetic manipulation,[92] in this case, the very discovery of ("irrational") PAP3 liposomes and the biological mechanism revealing the involvement of lipase-mediated pathways was only possible through our ability to screen and visualize large numbers of liposome formulations in vivo at high resolution and across an entire living organism.

4. Experimental Section

Liposome Formulation: Liposomes were formulated by extrusion or by ethanol injection (Note: DOPC:DOaG liposomes could be only formulated by ethanol injection) in ddH$_2$O at a total lipid concentration of 5 mM and containing 0.2 mol% DOPE-Lissamine Rhodamine (DOPE-LR) for fluores-

cent visualization unless otherwise stated. In the case of extrusion, individual lipids as stock solutions (1-10 mM) in chloroform, were combined to the desired molar ratios and dried to a thin film, first under an N$_2$ stream, then >1 h under vacuum. Lipid films were hydrated above the T_m of all lipids (65–70 °C), with gentle vortexing if necessary, to form a suspension. Large unilamellar vesicles were formed through extrusion (mini extruder, Avanti Polar Lipids) above the T_m of all lipids (i.e., 65–70 °C). Hydrated lipids were passed 11 times through 2 × 400 nm polycarbonate (PC) membranes (Nucleopore Track-Etch membranes, Whatman), followed by 11 times through 2 × 100 nm PC membranes. All liposomes were stored at 4 °C and used within 1 week.

In the case of ethanol injection, lipid films were re-dissolved in ethanol to a total lipid concentration of 50 mM. Using a glass micro-syringe (Hamilton, syringe series 700, volume 50 or 500 μl) 50 or 100 μL of the ethanolic solution was rapidly injected in a glass vial containing 0.5 mL or 1 mL ddH$_2$O, respectively, (1:10 v/v; EtOH:H$_2$O) at 70 °C under constant vigorous stirring (650 rpm – stirring bar dimensions: 12 × 4 × 4 cm), to form large unilamellar vesicles. Liposomes were then transferred to a dialysis tube (Spectrum labs, 3.5k MWCO) or a dialysis cassette (slide-A-Lyzer^{TM} 3.5k MWCO, Thermo Fisher Scientific) and dialyzed against ddH$_2$O overnight at 4 °C, to ensure complete ethanol removal. All liposomes were stored at 4 °C and used within 1 week.

Cryogenic Transmission Electron Microscopy and 3D Tomography: Liposomes (3 μL, 5 mM total lipid concentration) were applied to a freshly glow-discharged carbon 200 mesh Cu grid (Lacey carbon film, Electron Microscopy Sciences, Aurion, The Netherlands). Grids were blotted for 3 s at 99% humidity in a Vitrobot plunge-freezer (FEI VitrobotTM Mark III, Thermo Fisher Scientific). Cryo-EM images were collected on a Talos L120C or a KRIOS (NeCEN, Leiden University) operating at 120 or 300 kV, respectively. In the case of Talos, images were recorded manually at a nominal magnification of 17 500x or 28 000x yielding a pixel size at the specimen of 5.83 or 3.56 Å, respectively. In the case of KRIOS, images were recorded manually at a nominal magnification of 33 000x yielding a pixel size at the specimen of 3.48 Å. Alternatively, imaging and cryo-ET were performed on a Titan Krios operating at 300 kV (TU Eindhoven). Images were recorded manually at a nominal magnification of 6500x or 24 000x yielding a pixel size at the specimen of 13.87 or 3.86 Å, respectively. Tomographic tilt series acquisition was performed with Inspect3D software from Thermo Fisher Scientific with a total electron dose of less than 100 e nm^{-2}. Alignment and reconstruction of the series were performed using IMOD[93] and Avizo 9 (Thermo Fisher Scientific).

Zebrafish Husbandry and Injections: Zebrafish (*Danio rerio*, strain AB/TL) were maintained and handled according to the guidelines from the Zebrafish Model Organism Database (http://zfin.org) and in compliance with the directives of the local animal welfare committee of Leiden University. Fertilization was performed by natural spawning at the beginning of the light period, and eggs were raised at 28.5 °C in egg water (60 μg mL^{-1} Instant Ocean sea salts). The following previously established zebrafish lines were used: Tg(*cldn5a*:eGFP),[42] Tg(*kdrl*:eGFP)^{s843},[94] Tg(*mpeg1*:GFP)^{gl22},[95] Tg(*mpeg1*:mCherry)^{gl23},[95] and a previously generated zebrafish mutant (*stabilin-1*^{ibl3} *stabilin-2*^{ibl1}).[39] Liposomes were injected into 54–120 h post-fertilization zebrafish embryos using a modified microangiography protocol.[5] Embryos were anesthetized in 0.01% tricaine and embedded in 0.4% agarose-containing tricaine before injection. To improve the reproducibility of microangiography experiments, 1 nl volume was calibrated and injected into the sinus venosus/Duct of Cuvier or the primary head sinus. A small injection space was created by penetrating the skin with the injection needle and gently pulling the needle back, thereby creating a small pyramidal space in which the liposomes were injected. Successfully injected embryos were identified through the backward translocation of venous erythrocytes and the absence of damage to the yolk ball. More details about the protocol used or injections in the zebrafish embryo are provided in ref. [96]. Heparin (1 nl of 50 mg ml^{-1}) was injected 30 min before/after liposome injection. XEN445 (first dissolved in DMSO to obtain a 10 mM stock solution and then diluted in water to a final concentration of 50 μM) was administered 24 and 1 h prior to liposome injection.

**ADVANCED
SCIENCE NEWS**

www.advancedsciencenews.com

**ADVANCED
HEALTHCARE
MATERIALS**

www.advhealthmat.de

Confocal Imaging Acquisition and Editing: Zebrafish embryos were randomly picked from a dish of 20–60 successfully injected embryos. Confocal z-stacks were captured on a Leica TCS SPE or SP8 confocal microscope, using a 10x air objective (HCX PL FLUOTAR), a 40x water-immersion objective (HCX APO L), or 63x water-immersion objective (HC PL APO CS). For whole-embryo views, 3/4 overlapping z-stacks were captured to cover the complete embryo in lateral view. Laser intensity, gain, and offset settings were identical between stacks and each experiment. Images were processed and quantified using the Fiji distribution of ImageJ.[97,98] Confocal image stacks (raw data) are available upon request.

Studies on Mice: All experiments performed on mice were approved by the ethical committee of CIC biomaGUNE and by local authorities (Diputación Foral de Guipúzcoa), authorization number PRO-AE-SS-207, maintained and handled in accordance with the guidelines and regulations (Guidelines for Accommodation and Care of Animals). Male mice weighing ≈18–20 g (C57BL6, 6–8 weeks, Janvier; see below for the number of animals) were used. Animals were treated with 30 mg kg^{-1} XEN445 (as a suspension in 0.2% Tween-20/1% carboxymethyl cellulose) orally b.i.d. for 9 days[75] prior to liposome administration.

For radiolabeling studies, PAP3 liposomes (10 mM total lipid concentration) were made by ethanol injection as described above with the only difference that 0.2 mol% of NOTA-Bz-SCN-C18 (custom-made, Avanti Polar Lipids) was added to the lipid film. Additionally, the required total volume of liposomes was made in two batches of 500 µl to ensure avoidance of aggregation. After the formation of particles and removal of ethanol, $^{64}CuCl_2$ in 0.1 M aq. ammonium acetate pH = 5.5 was added to the liposome solution and the mixture was incubated at room temperature (20 mins) (1:4 v/v ammonium acetate/liposomes). Subsequently, the free $^{64}CuCl_2$ was removed by size exclusion chromatography (NAP^{TM}-25 columns Sephadex^{TM}, GE Healthcare) equilibrated with 10 mM tris buffer pH = 7.4. Elution fractions of 500 µl containing the radiolabeled liposomes were collected from the SEC column and their radioactivity was checked using a dose calibrator (CPCRC-25R, Capintec Inc., NJ, USA). The fraction containing the higher concentration of radioactivity was measured in size by DLS and was used for subsequent in vivo imaging and ex vivo studies.

For PET imaging studies, anesthesia was induced by inhalation of 3% isoflurane in pure O$_2$ and maintained by 1.5–2% isofluorane in 100% O$_2$. With the animal under anesthesia, the labeled liposomes were injected via one of the lateral tail veins (2845 ± 185 kBq/100 µl for treated animals; 2480 ± 260 kBq/100 µl for non-treated animals; $n = 2$ per group). Dynamic whole-body images (20 min duration) were acquired list-mode in a one-bed position in a 511 keV ± 30% energetic window immediately after administration of the labeled liposomes using a MOLECUBES β-CUBE scanner. Static 10 min images were also acquired at 2 and 6 h after administration. After each PET scan, whole-body high-resolution computed tomography (CT) acquisitions were performed on the MOLECUBES X-CUBE scanner, to provide anatomical information as well as the attenuation map for the later reconstruction of the PET images. Dynamic PET images were reconstructed with OSEM-3D iterative algorithm, using the following frames: 4 × 30, 4 × 60, 4 × 120, and 2 × 180 s. Static images were reconstructed as a single frame using the same method. Images were analyzed using π-MOD image analysis software (π-MOD Technologies Ltd, Zurich, Switzerland).

For ex vivo biodistribution studies, animals ($n = 3$ per compound and time point) were anesthetized with isoflurane 3% isoflurane in pure O$_2$ and maintained by 1.5–2% isoflurane in 100% O$_2$. A solution containing the labeled liposomes (2640 ± 370 kBq/100 µl for treated animals; 2530 ± 385 kBq/100 µl for non-treated animals; $n = 3$ per group and time point) was injected through one of the lateral tail veins. Animals were recovered from anesthesia and at pre-determined time points ($t = 10$ min, and 2, 6, and 24 h), animals were anesthetized again and sacrificed by perfusion using saline solution and brain, liver, kidneys, spleen, lungs, heart, and stomach were quickly removed and rinsed with water. The amount of radioactivity in each organ was measured in an automatic gamma counter (2470 Wizard, PerkinElmer). Blood samples were obtained just before perfusion. Part of the blood was processed to separate the plasma, which was also counted in the gamma counter. Results were normalized to injected dose and organ weight to express the results as a percentage of injected dose per gram of tissue (% ID/g).

Statistical Analysis: All experiments performed in zebrafish embryos/larvae presented in the main manuscript and in supporting information were repeated at least twice and were performed using freshly prepared liposomes. For all experiments performed in zebrafish, at least four embryos were randomly selected (from a pool of ≈20–60 successfully injected embryos) and visualized at low-resolution microscopy. From these four embryo/larva zebrafish, at least one was selected for confocal microscopy. The imaged zebrafish was representative of the data and showed consistent results confirming the presented data. No statistical analysis is performed in this work. Statistical analysis is as follows: for the ex vivo gamma radiation studies, results were normalized to injected dose and organ weight to express the results as a percentage of injected dose per gram of tissue (% ID/g). Data are presented as mean ± SD values. The sample size used for mice studies was $n = 2$ per group per time-point for the PET images and $n = 3$ per group per time point for the ex vivo gamma radiation experiments. Statistical significance was evaluated using a two-tailed unpaired Student's t-test. ns: not significant ($p > 0.05$). Significantly different *$p < 0.05$, **$p < 0.01$; ***$p < 0.001$. Exact p-values are included in the figure captions. GraphPad was used as software for the statistical analysis.

Supporting Information

Supporting Information is available from the Wiley Online Library or from the author.

Conflict of Interest

The authors declare no conflict of interest.

Data Availability Statement

The data that support the findings of this study are available from the corresponding author upon reasonable request.

[1] K. R. Feingold, Introduction to lipids and lipoproteins, in *Endotext* (Eds: K. R. Feingold, B. Anawalt, A. Boyce, G. Chrousos, W. W. de Herder, K. Dhatariya, K. Dungan, A. Grossman, J. M. Hershman, J. Hofland, S. Kalra, G. Kaltsas, C. Koch, P. Kopp, M. Korbonits, C. S. Kovacs, W. Kuohung, B. Laferrere, E. A. McGee, R. McLachlan, J. E. Morley, M. New, J. Purnell, R. Sahay, F. Singer, C. A. Stratakis, D. L. Trence, D. P. Wilson), MDText, South Dartmouth, MA **2000**.

[2] A. Akinc, M. A. Maier, M. Manoharan, K. Fitzgerald, M. Jayaraman, S. Barros, S. Ansell, X. Du, M. J. Hope, T. D. Madden, B. L. Mui, S. C. Semple, Y. K. Tam, M. Ciufolini, D. Witzigmann, J. A. Kulkarni, R. van der Meel, P. R. Cullis, *Nat. Nanotechnol.* **2019**, *14*, 1084.

[3] A. Akinc, W. Querbes, S. De, J. Qin, M. Frank-Kamenetsky, K. N. Jayaprakash, M. Jayaraman, K. G. Rajeev, W. L. Cantley, J. R. Dorkin, et al., *Mol. Ther.* **2010**, *18*, 1357.

[4] D. P. Schrijver, A. de Dreu, S. R. J. Hofstraat, E. Kluza, R. Zwolsman, J. Deckers, T. Anbergen, K. de Bruin, M. M. Trines, E. G. Nugraha, F. Ummels, R. J. Röring, T. J. Beldman, A. J. P. Teunissen, Z. A. Fayad, R. van der Meel, W. J. M. Mulder, *Adv. Ther.* **2021**, *4*, 2100083.

[5] C. Wolfrum, S. Shi, K. N. Jayaprakash, M. Jayaraman, G. Wang, R. K. Pandey, K. G. Rajeev, T. Nakayama, K. Charrise, E. M. Ndungo, T. Zimmermann, V. Koteliansky, M. Manoharan, M. Stoffel, *Nat. Biotechnol.* **2007**, *25*, 1149.

[6] B. A. Ference, H. N. Ginsberg, I. Graham, K. K. Ray, C. J. Packard, E. Bruckert, R. A. Hegele, R. M. Krauss, F. J. Raal, H. Schunkert, G. F. Watts, J. Borén, S. Fazio, J. D. Horton, L. Masana, S. J. Nicholls, B. G. Nordestgaard, B. van de Sluis, M.-R. Taskinen, L. Tokgözoglu, U. Landmesser, U. Laufs, O. Wiklund, J. K. Stock, M. J. Chapman, A. L. Catapano, *Eur. Heart J.* **2017**, *38*, 2459.

[7] J. L. Goldstein, M. S. Brown, *Cell* **2015**, *161*, 161.

[8] C. J. Fielding, P. E. Fielding, *J. Lipid Res.* **1995**, *36*, 211.

[9] C. M. Allan, N. H. Fidge, J. R. Morrison, J. Kanellos, *Biochem. J.* **1993**, *290*, 449.

[10] P. K. Vadiveloo, C. M. Allan, B. J. Murray, N. H. Fidge, *Biochemistry* **1993**, *32*, 9480.

[11] M. M. Hussain, D. K. Strickland, A. Bakillah, *Annu. Rev. Nutr.* **1999**, *19*, 141.

[12] Y. Shen, A. Lookene, L. Zhang, G. Olivecrona, *J. Biol. Chem.* **2010**, *285*, 7484.

[13] M. J. Amar, T. Sakurai, A. Sakurai-Ikuta, D. Sviridov, L. Freeman, L. Ahsan, A. T. Remaley, *J. Pharmacol. Exp. Ther.* **2015**, *352*, 227.

[14] H. Saito, S. Lund-Katz, M. C. Phillips, *Prog. Lipid Res.* **2004**, *43*, 350.

[15] S. Xu, M. Laccotripe, X. Huang, A. Rigotti, V. I. Zannis, M. Krieger, *J. Lipid Res.* **1997**, *38*, 1289.

[16] D. L. Williams, M. de La Llera-Moya, S. T. Thuahnai, S. Lund-Katz, M. A. Connelly, S. Azhar, G. M. Anantharamaiah, M. C. Phillips, *J. Biol. Chem.* **2000**, *275*, 18897.

[17] S. T. Thuahnai, S. Lund-Katz, G. M. Anantharamaiah, D. L. Williams, M. C. Phillips, *J. Lipid Res.* **2003**, *44*, 1132.

[18] A. Chroni, T. Liu, I. Gorshkova, H. Y. Kan, Y. Uehara, A. Von Eckardstein, V. I. Zannis, *J. Biol. Chem.* **2003**, *278*, 6719.

[19] N. Wang, D. L. Silver, P. Costet, A. R. Tall, *J. Biol. Chem.* **2000**, *275*, 33053.

[20] M. Denis, B. Haidar, M. Marcil, M. Bouvier, L. Krimbou, J. Genest, Jr., *J. Biol. Chem.* **2004**, *279*, 7384.

[21] M. Jaye, K. J. Lynch, J. Krawiec, D. Marchadier, C. Maugeais, K. Doan, V. South, D. Amin, M. Perrone, D. J. Rader, *Nat. Genet.* **1999**, *21*, 424.

[22] I. V. Fuki, N. Blanchard, W. Jin, D. H. Marchadier, J. S. Millar, J. M. Glick, D. J. Rader, *J. Biol. Chem.* **2003**, *278*, 34331.

[23] J. R. Mead, S. A. Irvine, D. P. Ramji, *J. Mol. Med.* **2002**, *80*, 753.

[24] P. W. Connelly, *Clin. Chim. Acta* **1999**, *286*, 243.

[25] K. Hirata, H. L. Dichek, J. A. Cioffi, S. Y. Choi, N. J. Leeper, L. Quintana, G. S. Kronmal, A. D. Cooper, T. Quertermous, *J. Biol. Chem.* **1999**, *274*, 14170.

[26] S. Santamarina-Fojo, K. A. Dugi, *Curr. Opin. Lipidol.* **1994**, *5*, 117.

[27] B. Landin, A. Nilsson, J. S. Twu, M. C. Schotz, *J. Lipid Res.* **1984**, *25*, 559.

[28] K. A. Dugi, H. L. Dichek, S. Santamarina-Fojo, *J. Biol. Chem.* **1995**, *270*, 25396.

[29] M. G. McCoy, G. S. Sun, D. Marchadier, C. Maugeais, J. M. Glick, D. J. Rader, *J. Lipid Res.* **2002**, *43*, 921.

[30] J. E. Yu, S. Y. Han, B. Wolfson, Q. Zhou, *Histol. Histopathol.* **2018**, *33*, 1.

[31] T. Ishida, S. Choi, R. K. Kundu, K. Hirata, E. M. Rubin, A. D. Cooper, T. Quertermous, *J. Clin. Invest.* **2003**, *111*, 347.

[32] M. E. Paradis, B. Lamarche, *Can. J. Cardiol.* **2006**, *22 Suppl. B*, 31B.

[33] W. Jin, J. S. Millar, U. Broedl, J. M. Glick, D. J. Rader, *J. Clin. Invest.* **2003**, *111*, 357.

[34] J. G. Strauss, R. Zimmermann, A. Hrzenjak, Y. Zhou, D. Kratky, S. Levak-Frank, G. M. Kostner, R. Zechner, S. Frank, *Biochem. J.* **2002**, *368*, 69.

[35] M. Merkel, Y. Kako, H. Radner, I. S. Cho, R. Ramasamy, J. D. Brunzell, I. J. Goldberg, J. L. Breslow, *Proc. Natl. Acad. Sci. U. S. A.* **1998**, *95*, 13841.

[36] S. Sieber, P. Grossen, P. Detampel, S. Siegfried, D. Witzigmann, J. Huwyler, *J. Controlled Release* **2017**, *264*, 180.

[37] G. Arias-Alpizar, L. Kong, R. C. Vlieg, A. Rabe, P. Papadopoulou, M. S. Meijer, S. Bonnet, S. Vogel, J. van Noort, A. Kros, F. Campbell, *Nat. Commun.* **2020**, *11*, 3638.

[38] F. Campbell, F. L. Bos, S. Sieber, G. Arias-Alpizar, B. E. Koch, J. Huwyler, A. Kros, J. Bussmann, *ACS Nano* **2018**, *12*, 2138.

[39] G. Arias-Alpizar, B. Koch, N. M. Hamelmann, M. A. Neustrup, J. M. J. Paulusse, W. Jiskoot, A. Kros, J. Bussmann, *Nanomedicine* **2021**, *34*, 102395.

[40] Y. Hayashi, M. Takamiya, P. B. Jensen, I. Ojea-Jiménez, H. Claude, C. Antony, K. Kjaer-Sorensen, C. Grabher, T. Boesen, D. Gilliland, C. Oxvig, U. Strähle, C. Weiss, *ACS Nano* **2020**, *14*, 1665.

[41] C. Quinonez-Silvero, K. Hubner, W. Herzog, *Dev. Biol.* **2020**, *457*, 181.

[42] L. M. van Leeuwen, R. J. Evans, K. K. Jim, T. Verboom, X. Fang, A. Bojarczuk, J. Malicki, S. A. Johnston, A. M. van der Sar, *Biol. Open* **2018**, *7*, bio030494.

[43] F. Ulrich, L. H. Ma, R. G. Baker, J. Torres-Vazquez, *Dev. Biol.* **2011**, *357*, 134.

[44] J. Zhang, M. Liss, H. Wolburg, I. E. Blasig, S. Abdelilah-Seyfried, *Ann. N. Y. Acad. Sci.* **2012**, *1257*, 193.

[45] J. Zhang, J. Piontek, H. Wolburg, C. Piehl, M. Liss, C. Otten, A. Christ, T. E. Willnow, I. E. Blasig, S. Abdelilah-Seyfried, *Proc. Natl. Acad. Sci. U. S. A.* **2010**, *107*, 1425.

[46] K. Ando, S. Fukuhara, N. Izumi, H. Nakajima, H. Fukui, R. N. Kelsh, N. Mochizuki, *Development* **2016**, *143*, 1328.

[47] D. A. Lyons, W. S. Talbot, *Cold Spring Harbor Perspect. Biol.* **2014**, *7*, a020586.

[48] R. A. Umans, H. E. Henson, F. Mu, C. Parupalli, B. Ju, J. L. Peters, K. A. Lanham, J. S. Plavicki, M. R. Taylor, *Dev. Biol.* **2017**, *425*, 101.

[49] N. M. O'Brown, S. G. Megason, C. Gu, *Elife* **2019**, *8*, 47326.

[50] S. Isogai, M. Horiguchi, B. M. Weinstein, *Dev. Biol.* **2001**, *230*, 278.

[51] M.-A. Moradi, P. H. H. Bomans, A. W. Jackson, A. M. van Herk, J. P. A. Heuts, *Eur. Polym. J.* **2018**, *108*, 329.

[52] M. A. Moradi, S. Tempelaar, A. M. van Herk, J. P. A. Heuts, *Macromolecules* **2019**, *52*, 9476.

[53] Y. Wu, S. Manna, P. Petrochenko, B. Koo, L. Chen, X. Xu, S. Choi, D. Kozak, J. Zheng, *Int. J. Pharm.* **2020**, *577*, 118998.

[54] A. K. Leung, Y. Y. Tam, S. Chen, I. M. Hafez, P. R. Cullis, *J. Phys. Chem. B* **2015**, *119*, 8698.

[55] M. L. Brader, S. J. Williams, J. M. Banks, W. H. Hui, Z. H. Zhou, L. Jin, *Biophys. J.* **2021**, *120*, 2766.

[56] H. De Boeck, R. Zidovetzki, *Biochemistry* **1989**, *28*, 7439.

[57] E. M. Goldberg, D. S. Lester, D. B. Borchardt, R. Zidovetzki, *Biophys. J.* **1994**, *66*, 382.

[58] A. M. Jimenez-Monreal, J. Villalain, F. J. Aranda, J. C. Gomez-Fernandez, *Biochim. Biophys. Acta* **1998**, *1373*, 209.

[59] F. M. Goni, A. Alonso, *Prog. Lipid Res.* **1999**, *38*, 1.

[60] J. A. Szule, N. L. Fuller, R. P. Rand, *Biophys. J.* **2002**, *83*, 977.

[61] P. Campomanes, V. Zoni, S. Vanni, *Commun. Chem.* **2019**, *2*, 72.

[62] T. M. Allen, C. Hansen, F. Martin, C. Redemann, A. Yau-Young, *Biochim. Biophys. Acta* **1991**, *1066*, 29.

[63] P. K. Working, M. S. Newman, S. K. Huang, E. Mayhew, J. Vaage, D. D. Lasic, *J. Liposome Res.* **1994**, *4*, 667.

[64] J. P. Otis, E. M. Zeituni, J. H. Thierer, J. L. Anderson, A. C. Brown, E. D. Boehm, D. M. Cerchione, A. M. Ceasrine, I. Avraham-Davidi, H. Tempelhof, K. Yaniv, S. A. Farber, *Dis. Models Mech.* **2015**, *8*, 295.

[65] R. L. Miyares, V. B. de Rezende, S. A. Farber, *Dis. Models Mech.* **2014**, *7*, 915.

[66] J. Y. Kim, J. Seo, K. H. Cho, *Food Chem. Toxicol.* **2011**, *49*, 2899.

[67] Y. Song, R. D. Cone, *FASEB J.* **2007**, *21*, 2042.

[68] S. Nishio, Y. Gibert, L. Bernard, F. Brunet, G. Triqueneaux, V. Laudet, *Dev. Dyn.* **2008**, *237*, 1682.

[69] J. L. Anderson, J. D. Carten, S. A. Farber, *Methods Cell Biol.* **2011**, *101*, 111.

[70] C. Liu, K. P. Gates, L. Fang, M. J. Amar, D. A. Schneider, H. Geng, W. Huang, J. Kim, J. Pattison, J. Zhang, J. L. Witztum, A. T. Remaley, P. D. Dong, Y. I. Miller, *Dis. Models Mech.* **2015**, *8*, 989.

[71] R. Pattipeiluhu, S. Crielaard, I. Klein-Schiphorst, B. I. Florea, A. Kros, F. Campbell, *ACS Cent. Sci.* **2020**, *6*, 535.

[72] C. Li, X. F. Tan, T. K. Lim, Q. Lin, Z. Gong, *Sci. Rep.* **2016**, *6*, 24329.

[73] D. P. Muller, T. R. Gamlen, *Pediatr. Res.* **1984**, *18*, 881.

[74] A. Ori, M. C. Wilkinson, D. G. Fernig, *J. Biol. Chem.* **2011**, *286*, 19892.

[75] S. Sun, R. Dean, Q. Jia, A. Zenova, J. Zhong, C. Grayson, C. Xie, A. Lindgren, P. Samra, L. Sojo, M. van Heek, L. Lin, D. Percival, J. M. Fu, M. D. Winther, Z. Zhang, *Bioorg. Med. Chem.* **2013**, *21*, 7724.

[76] P. K. Lo, Y. Yao, Q. Zhou, *Sci. Rep.* **2020**, *10*, 8911.

[77] Y. N. Zhang, W. Poon, A. J. Tavares, I. D. McGilvray, W. C. W. Chan, *J. Controlled Release* **2016**, *240*, 332.

[78] S. Wilhelm, A. J. Tavares, Q. Dai, S. Ohta, J. Audet, H. F. Dvorak, W. C. W. Chan, *Nat. Rev. Mater.* **2016**, *1*, 16014.

[79] R. Kuai, C. Subramanian, P. T. White, B. N. Timmermann, J. J. Moon, M. S. Cohen, A. Schwendeman, *Int. J. Nanomedicine* **2017**, *12*, 6581.

[80] M. Lameijer, T. Binderup, M. M. T. van Leent, M. L. Senders, F. Fay, J. Malkus, B. L. Sanchez-Gaytan, A. J. P. Teunissen, N. Karakatsanis, P. Robson, X. Zhou, Y. Ye, G. Wojtkiewicz, J. Tang, T. T. P. Seijkens, J. Kroon, E. S. G. Stroes, A. Kjaer, J. Ochando, T. Reiner, C. Pérez-Medina, C. Calcagno, E. A. Fisher, B. Zhang, R. E. Temel, F. K. Swirski, M. Nahrendorf, Z. A. Fayad, E. Lutgens, W. J. M. Mulder, et al., *Nat. Biomed. Eng.* **2018**, *2*, 279.

[81] M. M. T. van Leent, A. E. Meerwaldt, A. Berchouchi, Y. C. Toner, M. E. Burnett, E. D. Klein, A. V. D. Verschuur, S. A. Nauta, J. Munitz, G. Prevot, E. M. van Leeuwen, F. Ordikhani, V. P. Mourits, C. Calcagno, P. M. Robson, G. Soultanidis, T. Reiner, R. R. M. Joosten, H. Friedrich, J. C. Madsen, E. Kluza, R. vander Meel, L. A. B. Joosten, M. G. Netea, J. Ochando, Z. A. Fayad, C. Pérez-Medina, W. J. M. Mulder, A. J. P. Teunissen, *Sci Adv* **2021**, *7*, abe7853.

[82] G. Zhu, J. N. Mock, I. Aljuffali, B. S. Cummings, R. D. Arnold, *J. Pharm. Sci.* **2011**, *100*, 3146.

[83] M. Sharipov, S. M. Tawfik, Z. Gerelkhuu, B. T. Huy, Y. I. Lee, *Sci. Rep.* **2017**, *7*, 16073.

[84] J. C. Gomez-Fernandez, S. Corbalan-Garcia, *Chem. Phys. Lipids* **2007**, *148*, 1.

[85] M. Alwarawrah, J. Dai, J. Huang, *J. Chem. Theory Comput.* **2012**, *8*, 749.

[86] M. N. Holme, M. H. Rashid, M. R. Thomas, H. M. G. Barriga, K. L. Herpoldt, R. K. Heenan, C. A. Dreiss, J. L. Banuelos, H. N. Xie, I. Yarovsky, M. M. Stevens, *ACS Cent. Sci.* **2018**, *4*, 1023.

[87] P. J. Tacken, F. D. Beer, L. C. Vark, L. M. Havekes, M. H. Hofker, K. Willems Van Dijk, *Biochem. J.* **2000**, *347*, 357.

[88] B. Thisse, C. Thisse, ZFIN Direct Data Submission, **2004**.

[89] C. Liu, T. Han, D. L. Stachura, H. Wang, B. L. Vaisman, J. Kim, R. L. Klemke, A. T. Remaley, T. M. Rana, D. Traver, Y. I. Miller, *Nat. Commun.* **2018**, *9*, 1310.

[90] M. L. Lindegaard, J. E. Nielsen, J. Hannibal, L. B. Nielsen, *J. Lipid Res.* **2005**, *46*, 439.

[91] M. L. Lindegaard, G. Olivecrona, C. Christoffersen, D. Kratky, J. Hannibal, B. L. Petersen, R. Zechner, P. Damm, L. B. Nielsen, *J. Lipid Res.* **2005**, *46*, 2339.

[92] S. Sieber, P. Grossen, J. Bussmann, F. Campbell, A. Kros, D. Witzigmann, J. Huwyler, *Adv. Drug Delivery Rev.* **2019**, *151–152*, 152.

[93] G. C. Kemmer, S. A. Bogh, M. Urban, M. G. Palmgren, T. Vosch, J. Schiller, T. Gunther Pomorski, *Analyst* **2015**, *140*, 6313.

[94] S. W. Jin, D. Beis, T. Mitchell, J. N. Chen, D. Y. Stainier, *Development* **2005**, *132*, 5199.

[95] F. Ellett, L. Pase, J. W. Hayman, A. Andrianopoulos, G. J. Lieschke, *Blood* **2011**, *117*, 49.

[96] G. Arias-Alpizar, J. Bussmann, F. Campbell, *Bio-Protoc.* **2021**, *11*, 4173.

[97] J. Schindelin, I. Arganda-Carreras, E. Frise, V. Kaynig, M. Longair, T. Pietzsch, S. Preibisch, C. Rueden, S. Saalfeld, B. Schmid, J. Y. Tinevez, D. J. White, V. Hartenstein, K. Eliceiri, P. Tomancak, A. Cardona, *Nat. Methods* **2012**, *9*, 676.

[98] C. A. Schneider, W. S. Rasband, K. W. Eliceiri, *Nat. Methods* **2012**, *9*, 671.